EFFECT OF DOPING WITH RARE EARTH ELEMENTS ON STRUCTURE AND MAGNETORESISTANCE OF La(Ca)MnO_3 MANGANITES

by

SEVGİ POLAT ALTINTAŞ

THESIS SUBMITTED TO
THE GRADUATE SCHOOL OF NATURAL AND APPLIED SCIENCES
OF
THE ABANT İZZET BAYSAL UNIVERSITY
IN PARTIAL FULFILLMENT OF THE REQUIREMENTS FOR THE
DEGREE OF
MASTER OF SCIENCE
IN
THE DEPARTMENT OF PHYSICS

JUNE 2011

Approval of the Graduate School of Natural and Applied Sciences

Prof. Dr. Nihat Çelebi

Director

I certify that this thesis satisfies all the requirements as a thesis for the degree of Master of Science.

Prof. Dr. Kıvılcım Kılıç

Head of Physics Department

This is to certify that we have read this thesis and that in our opinion it is fully adequate, in scope and quality as a thesis for the degree of Master of Science.

Assoc. Prof. Dr. Cabir Terzioğlu

Supervisor

Examining Committee Members

1. Assoc. Prof. Dr. Cabir Terzioğlu .....

2. Assoc. Prof. Dr. Oğuz Üstün .....

3. Assist. Prof. Dr. Cihan Parlak .....

ABSTRACT

Effect of doping with Rare Earth elements on structure and Magnetoresistance of La(Ca)MnO_3 manganites

Sevgi Polat Altıntaş

Master of Science, Department of Physics

Supervisor: Assoc. Prof. Dr. Cabir Terzioğlu

June 2011, 53 pages

We have investigated the influence of Europium (Eu) doping on structural and magneto-electrical properties of $La_{0.7}Ca_{0.3}MnO_3$ compounds. In order to analyze the physical mechanism of a spin disorder system and study their relative evolutions, two samples of nominal compositions $(La_{0.7-x}Eu_x)Ca_{0.3}\ MnO_3$ ($x = 0.0$ and 0.1) have been elaborated and characterized. In addition to structural changes seen by this kind of doping, the magnetoresistance (MR) and resistivity are increased while the metal-insulator transition temperature is decreased. Comparing the experimental data with the theoretical models shows that in the metal-ferromagnetic region, the electrical behaviour of both samples is quite well described by a theory based on Kondo-like spin dependent scattering, electron-electron scattering, electron-phonon and electron-magnon scatterings. For the high temperature paramagnetic insulating regime, the adiabatic small polaron hopping model is found to fit well the experimental curves.

Keywords: Lanthanum based manganites, Magnetoresistance (MR), Metal-insulator transition, doping

ÖZET

La(Ca)MnO_3 manganitlerin yapısal ve Manyetodirenci üzerine Nadir Toprak Elementleri katkılamanın etkisi

Sevgi Polat Altıntaş

Yüksek Lisans, Fizik Bölümü

Tez Danışmanı: Doç. Dr. Cabir Terzioğlu

Haziran 2011, 53 sayfa

Europium (Eu) katkılamanın $La_{0.7}Ca_{0.3}MnO_3$ bileşiğinin yapısal ve manyeto-elektriksel özellikleri üzerine etkisini inceledim. Spin düzensiz bir sistemin fiziksel mekanizmasını analiz etmek ve göreceli evrimini çalışmak amacıyla, $(La_{0.7-x}Eu_x)$ $Ca_{0.3}$ MnO_3 ($x = 0.0$ ve 0.1) sembolik bileşikli iki numune ürettik ve karakterize ettik. Bu tip katkılamayla görünen yapısal değişikliklerin yanı sıra, manyeto-direnç ve özdirenç artarken metal-yalıtkan geçiş sıcaklığında azalma bulundu. Deneysel verileri teorik modellerle karşılaştırmamız gösterdi ki, metal-ferromanyetik bölgedeki elektriksel davranış Kondo-benzeri spine bağlı saçılma teorisi, elektron-elektron saçılması, elektron-fonon saçılması ve elektron-magnon saçılmalarıyla çok iyi açıklanabilir. Yüksek sıcaklık paramanyetik yalıtkan bölgede ise adyabatik küçük polaron sekme modeli deneysel eğrilerle çok iyi uyduğu bulundu.

Anahtar Kelimeler: Lanthanum bazlı manganitler, Manyetodirenç (MR), Metal-yalıtkan geçişi, katkılama

ACKNOWLEDGEMENTS

I express sincere appreciation to my advisor, Assoc. Prof. Dr. Cabir Terzioğlu for his guidance during my investigations, for the prompt and friendly help when needed, for his patient throughout this work and for his constructive remarks on the text.

This work was accomplished in cooperation with Assoc. Prof. Dr. Abderrezak Amira. My special gratitude to Amira for his valuable theoretical advise in various up-to-date solid state subjects and for the technical support during the research.

I also express sincere appreciation to Prof. Dr. Ahmet Varilci for his suggestions, contributions and his experience in laboratory. I would also like to say thanks to Assist. Prof. Dr. Cihan Parlak for the prompt and friendly help when needed. I am grateful for time spent with friends Ali Yılmaz and Gurcan Yıldırım and thank them for being great office mates.

I would like to thank my parents who have stood by me with strength until today and supported my pursuit to become a physicist. Finally, I would like to thank my husband Ferdi Altintas who has helped me countless times and supported me in all aspects of my life with love. Without his sacrifice and love, I could not come to this point. Needless to say, he is the most precious present I have ever received from God.

To My Parents...

TABLE OF CONTENTS

LIST OF FIGURES

LIST OF TABLES

CHAPTER 1

INTRODUCTION

In the past few decades, $AMnO_3$ perovskite-type manganites have been extensively analyzed because of their rich electrical transport and magnetic properties [1, 2, 3]. Considerable attention has been exposed from not only academic research but also magnetic industries. The growth of interest in their properties stems in large part from their wide range of technological applications such as read heads for magnetic information storage, low and high field magnetic sensors and more recently spintronic applications [4, 5, 6]. Numerous studies have been devoted in the rare earth manganite perovskite with the series of $(La_{1-x}RE_x)_{2/3}Ca_{1/3}MnO_3$ (RE is trivalent rare earth elements such as Y, Pr, Eu, Sm, etc) which are exhibiting colossal magnetoresistance (CMR) properties [7, 8]. These compounds are Mn^{3+} rich and doping with divalent atoms introduces mixture valency of Mn^{3+} and Mn^{4+} ions that plays a major role in the Double Exchange (DE) ferromagnetic interaction coupled with metallic resistivity [9]. Double exchange effect is an exchange of electrons from neighboring Mn^{3+} to Mn^{4+} ions through oxygen when their core spin are parallel. The hopping is not favored when they are anti-parallel. Although, more elucidative mechanisms need to explain the observed high magnitude of magnetoresistivity, such as polaronic effects, intrinsically inhomogeneous states and Jahn-Teller (JT) distortion [10, 11, 12, 13, 14, 15].

According to the literature, it was reported that the partial substitution of La^{3+} by Tb^{3+} in $La_{0.7}Ca_{0.3}MnO_3$ causes sharp changes in the magnetic and electrical properties [16]. Also, the substitution by Y^{3+} or Pr^{3+} decreases the Curie temperature and enhances the resistivity of the samples [17, 18]. The effect of Eu doping at A-site of manganites has been studied by many groups. In fact,

Reddy *et al.* [19] showed that the Eu doped $La_{0.67-x}Eu_xCa_{0.33}MnO_3$ compounds with $x \leq 0.29$ exhibit lower Curie and insulator-metal transition temperatures with respect to the undoped sample in addition to possessing CMR property. Similar results have been reported too by several groups in Sm, K and Gd doped CMR manganites [20, 21, 22].

In this thesis and for a better understanding of the effect of Eu doping on structural and magneto-electrical properties of lanthanum based compounds, we have elaborated and characterized two samples of nominal compositions $La_{0.7-x}Eu_x$ $Ca_{0.3}MnO_3$ (x=0 and 0.1) [23]. This is a typical example of a spin-disorder system and is suitable from studying the physical mechanisms and their relative evolutions. In addition to structural changes seen by this kind of doping, an increase in resistivity and a decrease of the metal-insulator transition temperature are revealed. As observed in recent studies [24, 25, 26, 27], a minimum in resistivity was also obtained in the present work. In order to explain the origin of this behavior, the experimental data is analyzed by using different mechanisms, such as spin dependent transport mechanism, Kondo like scattering and quantum correction to conductivity [28, 29, 30]. Although there are many works including the physical mechanism of the low temperature resistivity minimum, it needs further clarifications for a deeper understanding. At high temperatures, the semi-conducting-like curve resistivity is fitted by the small polaron hopping (PH) model and the nature of the conduction is inferred.

Morover, in order to analyze the conduction mechanism in the entire temperature region, we focused on the study of resistivity as functions of temperature and magnetic field, and intended to elucidate the role of competition between the FM and PI phases. It was approximated that the two main separated phases coexist in the doped perovskite manganese oxides: one is the paramagnetic insulating phase, and the other is the ferromagnetic metallic phase, with the energy difference to form the two phases. Under this approximation, the temperature dependence of the volume fraction distribution is supposed to follow the Boltz-

man distribution of a two energy-level system, then we used a simple model to describe the PI-FM transition and CMR.

1.1 Characteristics of Perovskite Manganites

The $R_{1-x}A_xMnO_3$ perovskite manganites, where R and A are some rare earth and alkaline earth elements respectively and $0.2 < x < 0.5$, display the unusual property of being paramagnetic insulators at high temperatures and ferromagnetic metals at low temperatures [31, 32, 33, 34]. Perovskite is the name of the structure type, Figure 1.1, containing corner sharing MnO_6 octahedra. Both end members of $La_{1-x}A_xMnO_3$ are antiferromagnetic insulators [35], but become ferromagnetic metals upon doping. The theory of double exchange [9, 36, 15] has been developed in order to explain this phenomenon and correctly predicts $x = 1/3$ to be optimal doping [37]. Recent calculations show that a second mechanism such as a Jahn-Teller distortion may be required to explain the magnetoresistance within the double exchange model [13, 38, 39].

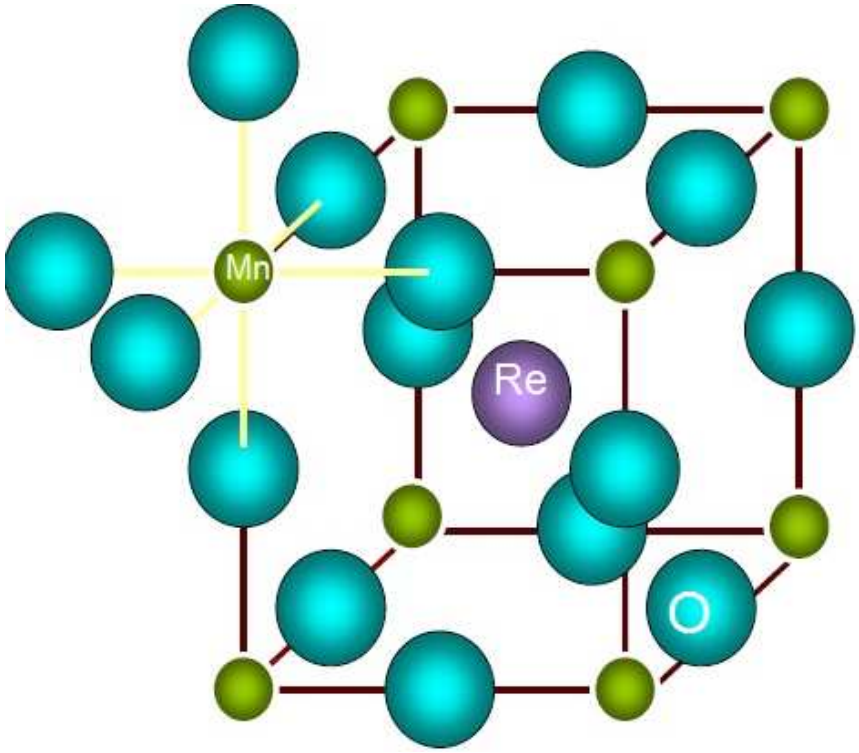

Figure 1.1: Model for the perovskite manganite of $Re^{3+}Mn^{3+}O_3^{2-}$. Re indicates a rare earth material, Mn indicates manganese and O indicates oxygen.

Until recently, much of the experimental work on the manganites has been motivated by their utility as magnetic recording devices, magnetic actuators, cathode materials in solid oxide fuel cells, etc. [40, 22, 41, 42]. Thus many compounds of the type $R_{1-x}A_xMnO_{3+\delta}$ have been studied in polycrystalline form [43, 44, 45, 46]. Much has been learned about their defect chemistry and high temperature electronic and ionic conductivity. Most of these compounds are not metallic above room temperature but have electronic conductivity, presumably due to (small) polaron hopping, sufficient to make good electrodes.

1.2 Important interactions in Manganites

1.2.1 Double Exchange Mechanism

The correlation between the electrical conductivity and ferromagnetism was introduced by Jonker and Van Santen [31] through the theory of double exchange proposed by Zener [9]. This theory predicts that, an electron may be exchanged between two species and has important implications for whether materials are ferromagnetic, antiferromagnetic or neither with relative ease. In the double exchange phenomenon $Mn^{3+}-O-Mn^{4+}$ and $Mn^{4+}-O-Mn^{3+}$ bonds degenerate leads to delocalization of the electron on Mn^{4+} site. The delocalization of electron at Mn^{4+} site lowers the energy of system and there is an energy gain by aligning the t_{2g} spins. The delocalization of electron at Mn^{4+} site can be shown as Fig. 1.2.

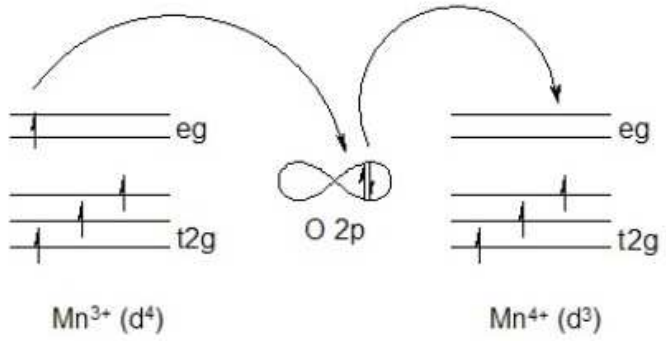

Figure 1.2: Representation of Double Exchange Mechanism.

Later Anderson and Hasegawa [36] calculated the hopping probability for a

more general alignment of the core spins by introducing a quantum mechanical view and it was shown that the conductivity and angle between core spins are related by $\cos(\theta/2)$ when θ indicates the relative angle between two manganese core spins. This double exchange mechanism gives an explanation of the relationship between magnetism and electron conductivity and it is proven by the experiment as shown in Fig.1.3. It is clearly shown for the mixed-valent manganese oxide $La_{1-x}Ca_xMnO_3$ that the ferromagnetic state is directly related to the conducting state of this material. The relationship, as explained by the double exchange mechanism, between the conductivity and Mn-Mn distance in the ferromagnetic metallic region is not sufficient to deal with systems with different A-site cations. The relationship in these systems could be partially explained by introducing the tolerance factor $t = (r_{Mn} + r_O)/(r_{Asite} + r_O)$, where r_{Mn}, r_O, and r_A site indicate the averaged ionic size of Mn, oxygen, and the A site cation respectively. This was shown by the experiment concerning manganites with a different A site cation radii with a fixed doping ratio [17]. This correction is necessary because of the Mn-O-Mn bond angle dependent T_c due to the effect of Jahn-Teller distortion.

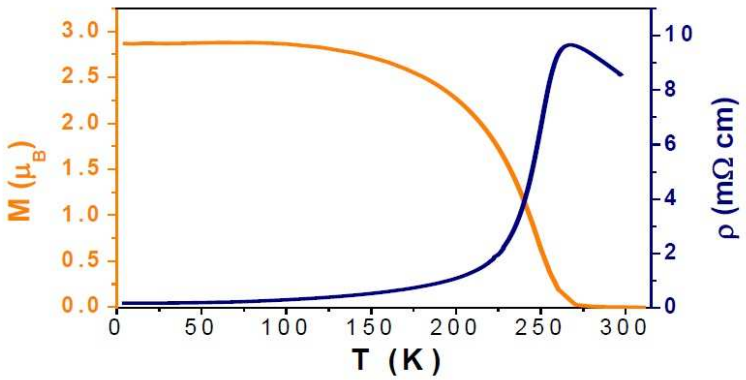

Figure 1.3: Magnetization and resistivity of the LCMO film. It shows the coexistence of the ferromagnetic phase with the metallic phase and the insulating phase with paramagnetic phase, which supports the double exchange mechanism.

1.2.2 A Mechanism in Addition to Double Exchange: Electron-Phonon Coupling

Phenomena such as the existence of the ferromagnetic insulating state, different types of orderings which are related to the different phases, the phase transition between different states or the coexistence of those phases states etc. are difficult to explain only by the double exchange mechanism. Therefore, a further explanation of the orderings and related phases and their dynamics for this mixed valent perovskite manganite is needed.

Figure 1.4 [47] shows one possible origin of the new mechanism. This phase diagram strongly suggests that the effect of the electron-lattice coupling by showing distinctive characteristic features in phases with a doping ratio, x, that is a multiple of 1/8 other than $x = 0.25$ and 0.75. The electron-lattice coupling is directly related to the polaron formation, which is induced by the trapping of charge carriers due to Jahn Teller distortion of the MnO_6 octahedron [13] and this is confirmed by the observation of the local Jahn Teller distortion (so called on site small polaron) in the metallic phase of $La_{1-x}Sr_xMnO_3$ ($0 < x < 0.4$) using pulsed neutron scattering [48]. The competition between this electron-phonon coupling and double exchange is considered to be the source of intrinsic phase separation in perovskite manganites. This electron-lattice coupling induces the charge ordered phase and orbital ordered phase, which can also be the dominant phases in manganites.

1.2.3 A Mechanism in Addition to Double Exchange: Disorder and Strain

Manganites are not a perfect crystal. Therefore, considering the effect of disorder in this material, especially, for mixed valence manganites is very appropriate. In addition to this, as a strongly correlated electron system, structural strain can affect other properties of manganites as well. Disorder in this material is

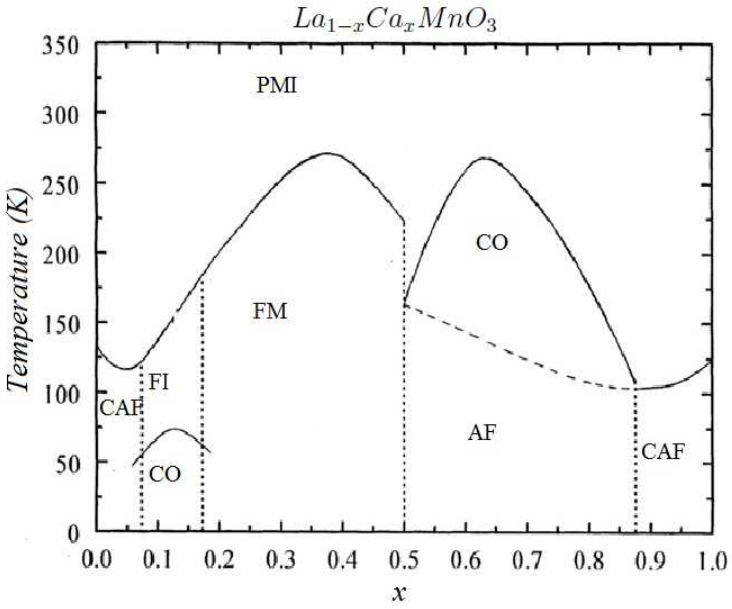

Figure 1.4: Phase diagram for $La_{1-x}Ca_xMnO_3$. CAF, FI, CO, FM and AF indicate Canted antiferromagnetic, Ferromagnetic insulating, Charge ordered, Ferromagnetic and antiferromagnetic respectively [47].

expected to suppress the mobility of the electrons and as a result it is expected to decrease the T_c and/or increase the residual resistivity [49] or suppress the magnetoresistance [50]. It is necessary to pay attention to the methods used to introduce disorder into the system to understand its mechanism. One possible way is by changing the doping ratio from the canonical double exchange system, $La_{0.7}Sr_{0.3}MnO_3$, i.e. modifying the A-site ionic valences to control the electron density. The second way to control disorder is by using a different growth mode including oxygen annealing and using different substrates. This can induce different structural symmetry and/or different structural strain [52]. The third way is by changing the chemical pressure by substituting a doping component Sr to Ca or Ba with a fixed doping ratio $x = 0.3$. This results in a modification of the length and angle of the Mn-O-Mn bonds and in this case the disorder can be quantified as the variation of the radius of the A-site cation ($\sigma^2 =< r^2 > - < r >^2$) [49, 50, 52]. We will call the disorder induced using the methods discussed above "intrinsic disorder". Due to the fact that experiments, in which this kind of intrinsic disorder is introduced, cannot distinguish between the effects of pure disorder and those of the strain itself, the role of disorder in the system, that is whether it

acts as a scattering source for mobile electrons or magnons due to the presence of localized corresponding states [52] or it accommodates built in strain to localize electrons assisted by Jahn-Teller distortion, is not yet clear [50].

1.2.4 Jahn-Teller (JT) Distortion

In the manganites the presence of the Mn^{+3} produces the Jahn-Teller (JT) effect [51], that affects the crystalline structure and the physical properties of the materials.

The electronic configuration of Mn^{3+} is $t_{2g}^3 e_g^1$, that is characterized by the presence of a single electron in the two-fold degenerate e_g level. As such, Mn^{3+} is a Jahn-Teller active chemical species. According to the Jahn-Teller theorem, the $Mn^{3+}O_6$ groups in $RE_{1-x}AE_xMnO_3$ are energetically unstable towards distortions aiming to reduce the total energy of the system, as a consequence of a lifting of degeneracy of the e_g levels. The degree of distortion is determined by the competition between the gain in energy due to the e_g splitting and the increase of the elastic energy associated to the lattice distortion itself.

Supposing that the octahedra distorts elongating, for example, along z-axis. The crystalline field has no more a cubic symmetry around the Mn ion, and the energies of the $d_{x^2-y^2}$ and d_{xy} orbital increase, because they result closer to the p oxygen orbitals. On the contrary, the energy of the d_{z^2} , d_{xz} and d_{yz} orbitals decreases, because they are further from the p oxygen orbitals as showed in Figure 1.5. The distort system has a lower electronic energy, but a higher elastic energy caused by the deformation. Therefore, the system tends to distort spontaneously if the gain in electronic energy is greater than the loss in elastic energy. This distortion is termed Jahn-Teller effect.

1.2.5 Orbital and Charge Ordering

The orbital ordering consists in a spatially ordered arrangement of d orbitals in the crystal. Strongly associated with the carrier concentration, it develops when

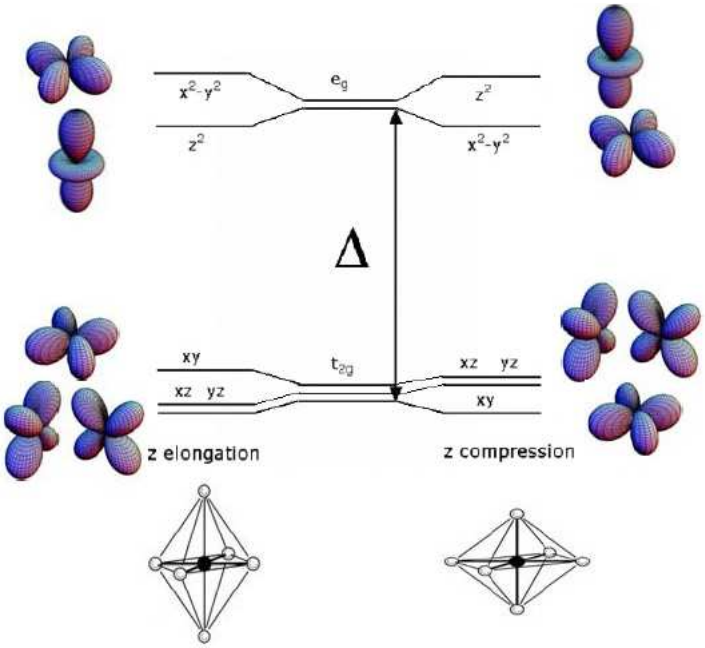

Figure 1.5: Jahn-Teller effect on d energy levels in the case of elongation (on the left) and of compression (on the right) along z direction of the $Mn^{3+}O_6$ octahedra [51].

the d electron occupies an asymmetric orbital. The direct electrostatic repulsion of the charge clouds, coupled with cooperative JT distortions, stabilizes the effect generating an ordered sublattice of orbitals.

The ratio Mn^{3+}/Mn^{4+} is responsible for the phenomenon of charge ordering (CO). This consists of a periodic distribution of electric charge (i.e. eg electrons of Mn^{3+} ions in the crystal lattice), driven by Coulomb interaction. The mobile e_g electrons may become localized at certain Mn ion positions in the lattice, forming an ordered sublattice. In principle, however, these charges do not need to be necessarily localized on the Mn sites, and in fact they could sit on the bond centres as well, or, in the most general case, on some intermediate point between those two. Such an intermediate CO state can be more generally seen as a charge-density wave, lacking inversion symmetry and then potentially capable to develop ferroelectric ordering.

CO is mainly observed at special concentration of dopant, namely at rational fractions (as for example $x = 1/8, 3/10, 1/2, 3/4$). In this case the extra electron of Mn^{3+} are localized on alternate manganese ions, creating an ordered path of

charge in the lattice. The CO can be either long-ranged or short-ranged. It is clear that CO is competitive with the electron conductivity, because it tends to inhibit the movement of the charges through the crystal. Compounds with long-range CO are generally insulating, but localised CO (polarons) is responsible for an enhancement of resistivity, introducing scattering centers for the mobile electrons.

1.2.6 Indirect Exchange Interaction: Superexchange

Superexchange is an indirect exchange interaction between non-neighbouring magnetic ions, which is mediated by a non-magnetic ion, that is placed in between them. This interaction was first proposed by Kramers [53] in 1934 to the aim of finding an explanation for the magnetic properties observed in insulating transition metal oxides, in which the magnetic ions are so distant that a direct exchange interaction could not explain the presence of magnetically ordered states, so the longer-range interaction that is operating in this case should be "super". The problem was thereafter treated theoretically by Anderson [36], who in 1950 gave the first quantitative formulation showing that the superexchange favours antiferromagnetic order.

1.3 $LaCaMnO_3$

In this thesis we have studied $La_{1-x}Ca_xMnO_3$ (LCMO) manganite doped at x = 0.3 ($La_{0.7}Ca_{0.3}MnO_3$). Therefore, further discussions of manganite properties will be restricted to LCMO system only. LCMO is the member of the perovskite family $R_{1-x}A_xMnO_3$, where $R = La$ and $A = Ca$.

Mn ions occupy the B-site of the ABO_3 perovskite structure at the center of the unit cell and are octahedrally coordinated by the oxygen ions. Adjacent MnO_6 octahedra are linked at their vertices. The La^{3+} and Ca^{2+} ions are then distributed randomly over the A-sites in the crystal. The cubic unit cell (shown in Fig.1.1) is idealized and is only seen at high temperature, above $\sim 1000\ K$, where

most perovskites are cubic. As the temperature is lowered, the MnO_6 octahedra distort and rotate around the oxygen links, thereby reducing the symmetry of the LCMO system. Below 700 K the structure remains orthorhombic Pnma, for calcium doping $x < 0.5$ and in some regimes for $x > 0.5$; and, therefore, the LCMO system can be studied in the absence of structural phase transitions. Simple perovskite compounds, i.e. $LaMnO_3$ and $CaMnO_3$ are insulators.

The primary electronic conduction in manganites occurs via the conduction band formed from the overlap of the Mn 3d and O 2p orbitals. The degree of overlap is maximized for a cubic perovskite structure (structure factor=1). Any deviations from this, either by lengthening or bending the Mn-O-Mn bond, will reduce the orbital overlap and the hopping amplitude of the itinerant e_g electron. It is possible to investigate the effects of chemical pressure on the Mn-O-Mn bond by substituting trivalent ions of differing sizes into the perovskite structure while keeping the fraction of divalent ions constant. Crucially this ionic substitution will leave the valency of the manganese ions and the number of potentially itinerant electrons unaltered.

LCMO has attracted a lot of interest, since it remains orthorhombic for all values of x, permitting different electronic and magnetic phases to be stable and coexist. The magnetic properties of manganites are largely determined by transfer of electrons between manganese and oxygen orbitals that point towards each other. This leads to series of current/electric field induced effects, and persistence of various transport mechanisms at different temperatures and doping levels. A vast amount of experimental work have been performed to explore the colossal magneto resistive CMR effect in different types of manganites. There is a growing consensus among researchers that phase separation (PS) can be directly responsible for the CMR effect in manganites system [54, 55, 56, 57].

1.4 Conduction mechanisms in LCMO

1.4.1 Hopping regime

In the high temperature regime at $T > T_C$, LCMO is usually a paramagnetic insulator (PMI). In this regime, electric conductivity is governed by electrons hopping through a dielectric insulator. There are three major possible mechanisms for conduction in this regime, each supported by some experimental evidence: i) thermally activated hopping model [58], ii) the nearest neighbours hopping model [59] and iii) a variable range hopping (VRH) model [60]. Since the experimental observations are carried out in a narrow temperature range just above T_C it is sometimes very difficult to distinguish between three mechanisms. Consequently, there is no agreement as to which mechanism actually prevails.

Thermally activated carriers

In this model, the carriers are thermally excited across the band gap from the valence bandto a conduction band. The resistivity ρ follows the Boltzmann law, as shown in equation 1.1, where E is the energy gap and ρ_∞ is the resistivity at temperature increasing to infinity.

$$\rho = \rho_\infty exp(\frac{E}{k_B T}) \tag{1.1}$$

This simple model is based on the resistivity given by $\rho = (ne\mu)^{-1}$, where n is the carrier density in the conduction band, e is the charge of an electron and μ is the carrier mobility. The dominant factor is normally the thermally activated form of n, and μ is assumed to be independent of temperature. It would be reasonable for the mobility to show some temperature dependence, which would introduce additional factors into equation 1.1.

If the conduction mechanism in the insulating paramagnetic and charge-ordered phases is due to thermally activated carriers, then the activation energy

should be different for different phases. A transition from the paramagnetic to charge-ordered states would then show up via a sudden change of gradient in the logarithm of resistance versus temperature.

Nearest neighbour hopping

In the paramagnetic state e_g electrons are thought to be associated with lattice distortions (i.e. they form polarons). Electrical conduction proceeds via polaron motion. In this model, the lattice distortions are of a size similar to unit cell size and the polarons move between the nearest neighbour sites. The resistivity in this case is given by:

$$\rho = ATexp(\frac{E}{k_BT}) \tag{1.2}$$

where A is a constant and E is the energy required to move a polaron.

However, the strong electron-polaron coupling seen in the $La_{1-x}Ca_xMnO_3$ means that the motion of the charge-carriers is slow compared with the lattice vibration. The motion of the electrons and the lattice cannot be separated, analysis in a non-adiabatic limit is more complicated [61] and the resistivity is given by:

$$\rho = AT^{3/2}exp(-\frac{E}{k_BT}) \tag{1.3}$$

Variable range hopping

If the activated energies for hopping to neightbouring atoms are not the same, then it may be that hopping to a non-nearest neighbour has a smaller activation

energy. This is particularly true at low temperatures [62]. This variable range hopping is more complicated to describe [61], but it can be summarized to:

$$\rho = \rho_{\infty} exp(\frac{T_0}{T})^{1/4} \tag{1.4}$$

where T_0 is a characteristic temperature.

One drawback of VRH models is that the values of T_0 are often implausibly high [63]. Another problem is that VRH was originally proposed for short distance (localization length l_{VRH}) hopping at low temperatures. There is further complication in that, the mechanism may depend on the type of the sample (single crystal, polycrystalline or thin film) [64]. VRH is assumed to be a dominant mechanism for electronic conduction in bulk noncrystalline insulating solids. As the distance of hoping grows $l > l_{VRH}$, direct tunneling becomes a dominant conduction process. With increasing barrier thickness, the conductance becomes temperature and bias dependent [65, 66].

1.4.2 Percolation regime

At temperature $T = T_C$, where T_C is a Curie temperature, PM phase turns into ferromagnetic (FM). In LCMO system the same temperature happens to be also a Metal-Insulation (M-I) transition temperature $T = T_{MI}$, where the insulating phase turns to a metal like one. Therefore, in our sample we have $T = T_C = T_{MI}$ and the PMI phase observed in high temperature turns into ferromagnetic metallic (FMM) state. The transition leads to a percolation metallic-like conductivity in the FM state. With decreasing temperature, more FM clusters are formed, enhancing percolation paths. The behavior of the resistivity ρ is expected to follow:

$$\rho \infty (p - p_c)^{-t} \tag{1.5}$$

where p is the concentration of the metallic phase, p_c is the critical concentration and t is the critical exponent of the resistivity.

In the vicinity of the transition, the metallic concentration is proportional to magnetization, which is approximately a linear function of $(T_C - T)$. Hence, instead of concentration, we can use $(T_C - T)$, which will result equation 1.5 to follow the power law:

$$\rho \infty (T - T_c)^{-t} \tag{1.6}$$

With more temperature decreasing, the intense competition between FMI and FMM phases gives rise to appearance of intrinsic tunnel barriers, interrupting metallic percolating paths. The dominant conduction mechanism crosses over, as a function of barrier thickness (hoping length), from a directed hopping, seen in FM regime, through resonant and direct tunneling, to indirect, inelastic tunneling. Low temperature resistivity is dominated by tunneling across intrinsic barriers.

1.5 Colossal Magneto Resistance

Colossal magnetoresistance is a materials property which enables it to change its electrical resistance in the presence of magnetic field. A magnetic field applied to perovskite manganite in the paramagnetic semiconducting state, enables its phase transformation into ferromagnetic metallic state causing colossal magnetoresistance to occur. The magnetoresistance has a peak close to position of the maximum slope of the resistivity curve. There should be a large change of resistivity with temperature to have a large magnetoresistance. Also the transition temperature should be highly sensitive to the applied field.

In doped manganites $RE_{1-x}AE_xMnO_3$ the origin of the CMR is connected with the presence of a metal-insulator transition. The CMR effect is observed in

manganites of a narrow range of composition between $x = 0.3$ and 0.4, where the coexistence of two micrometric magnetic phases in the absence of the magnetic field exists: a ferromagnetic insulating phase and an antiferromagnetic insulating one are observed. In the presence of a magnetic field, these phases transform into a ferromagnetic metallic phase at a Curie temperature T_C. The maximum effect of the CMR appears near the T_C. The magnetoresistance is usually defined as:

$$MR(\%) = \frac{|\rho(0) - \rho(H)|}{\rho(0)} \times 100, \tag{1.7}$$

where $\rho(0)$ and $\rho(H)$ are the measured resistivity without and with magnetic field, respectively.

Resistivity measurements versus temperature and applied magnetic field for the CMR $La_{0.67}Ca_{0.33}MnO_3$ single crystals are shown in figure 1.6.

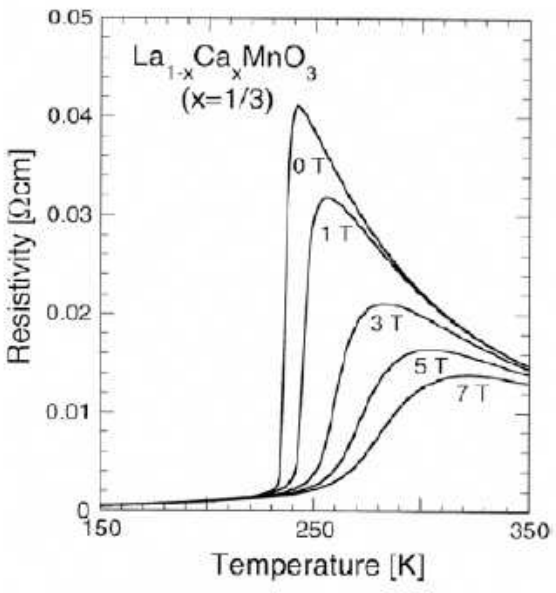

Figure 1.6: CMR behavior for the $La_{0.67}Ca_{0.33}MnO_3$ single crystal [67].

The double exchange phenomenon helps to explain the CMR effect. The applied magnetic field will align the t_{2g} spins and the transport will be possible between Mn+ ions. At the Curie temperature both spin will disorder and magnetic susceptibility will be high that maximizes the effect of applied field. In order to have a sharp transition between the metallic and insulating state, the

sample should be as homogeneous as possible so that all parts have the same transition temperature. If there are polycrystalline grains, there will be regions between the grains that have different transition temperatures because the material is distorted with different Mn-O-Mn bond angles and lengths and different Mn^{4+} concentrations. The resistivity curve for the whole sample is a superposition of the resistivity curves for the different parts, and with different transition temperatures there will be a broader transition.

Within the framework of the models proposed to explain the origin of CMR in manganites, I should mention the recently proposed percolation mechanism [54, 68]. This model is based on the idea that the colossal magnetoresistance is due to percolation between nanoscale ferromagnetic metallic (FMM) clusters in an antiferromagnetic insulating (AFI) matrix [69].

CHAPTER 2

EXPERIMENTAL

2.1 Sample Preparation

The most widely used method for preparing polycrystalline oxides is the direct reaction, in the solid state, of a mixture of solid starting materials. Powder solids are formed which can then be pressed and sintered to form dense polycrystalline pellets. Even though the desired phase is thermodynamically favored, solids do not usually react together at ambient temperature over laboratory time scales and it is necessary to heat the reactants at high temperatures to overcome the kinetic barriers. For such reactions, the rate limiting step is usually the solid state diffusion of the cations across the interface between the starting materials.

The bulk samples of $La_{0.7}Ca_{0.3}MnO_3$ and $La_{0.6}Eu_{0.1}Ca_{0.3}MnO_3$ are prepared by the conventional solid-state reaction method [23]. The highly purified powders (99.9 %) of La_2O_3, Eu_2O_3 , $CaCO_3$ and MnO_2 are mixed in stoichiometric ratios, ground and calcined at 1173 K for 20 h. The remaining black powder was ground, pelletized and sintered for another 20 h at 1273 K with two intermediate grindings. Finally the obtained pellets are reground, pelletized and annealed at 1423 K for 10 h. The $La_{0.6-x}Eu_xCa_{0.3}MnO_3$ sample synthesis procedure by the solid-state reaction is shown in Fig.2.1.

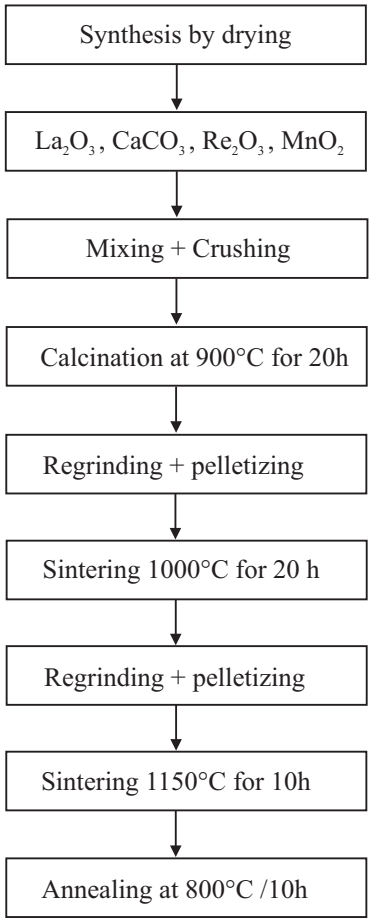

Figure 2.1: The $La_{0.7-x}Re_xCa_{0.3}MnO_3$ sample synthesis procedure by the solid-state reaction method.

2.2 Structural and Electro-transport Measurements

The phase purity and crystal structure are examined by X-Ray Diffraction (XRD) using a D 8-Advance Bruker type diffractometer with CuK_α radiation ($\lambda =$ 1.5418 Å). The cell parameters are refined by use of JANA2006 software [70].

The surface morphologies of the bulk samples were studied by using a JEOL JSM-6390LV scanning electron microscope (Fig. 2.2). SEM micrographs were taken from fracture surfaces of the bulk samples. Micrographs of the samples were magnified approximately 3000 times. We investigated microstructure of the sample, connectivity and size of the grains.

A standard technique to measure resistivity is typically referred to as a Van der Pauw four-point measurement. A current is applied to the sample across two adjacent contacts, and the voltage drop across the material is measured using the

Figure 2.2: JEOL JSM-6390LV Scanning Electron Microscope.

other two contacts (see Fig. 2.3). From knowledge of the current applied and a geometric factor involving the arrangement of the contacts one may convert the voltage measurement directly into a resistivity value. It is best if the current is kept constant, so that changes in voltage truly represent changes in resistivity.

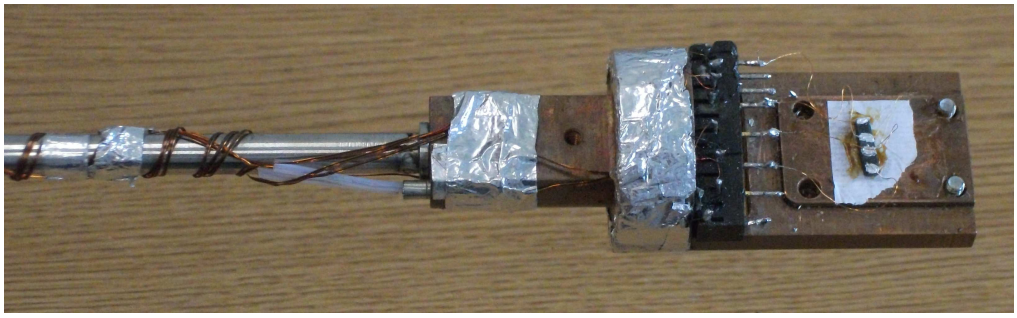

Figure 2.3: Experimental set-up for the 4-point probe measurement.

Resistivity measurements are carried on a He gas contact crycooler (see Fig. 2.4) and superconducting coil magnet in different applied fields $(0 - 7\ T)$over a temperature range $5 - 300\ K$.

Figure 2.4: He gas contact crycooler and superconducting coil magnet from CRY Industries.

CHAPTER 3

RESULTS AND DISCUSSION

3.1 Structural aspects

The X-ray diffraction patterns of all samples were recorded at room temperature and are displayed in Figure 3.1 [23]. Significant peaks that representing different hkl planes had been observed from the XRD patterns of LCMO and LECMO. One can see from the XRD patterns that the samples are well crystallized in a single phase since no extra peaks are detected. The observed lines of both samples belong to the simple-perovskite-type structure and are in agreement with previous results [71]. The superposition of the observed and calculated XRD patterns for both samples is shown in the insets of Figure 3.1. The refinement of cell parameters was done in the orthorhombic system with Pbnm space group. Details of the procedure are as follows. The experimental intensities are fitted by use of pseudo-Voight function. A 36 terms of Legendre polynoms was used to describe the backround and the Simpson method was applied for the asymmetry correction. The obtained cell parameters as well as the agreement factors (R_p, R_{wp}) and the goodness of the fit (GOF) are listed in Table 3.1. As can be seen, the GOF values for LCMO and LECMO were found to be 1.07 and 1.08, respectively. It is well known that when GOF value is ~ 1, the fitting is expected to be very good. The decrease of the cell volume with doping may be associated to the low ionic radii of Eu^{3+} (1.120 Å) than that of the substituted La^{3+} (1.216 Å) [72].

The representative SEM micrographs with 3000x magnification obtained at room temperature for LCMO and LECMO composites are shown in Figure 3.2 [23]. Overall, SEM images show that various sizes of grains are randomly distributed

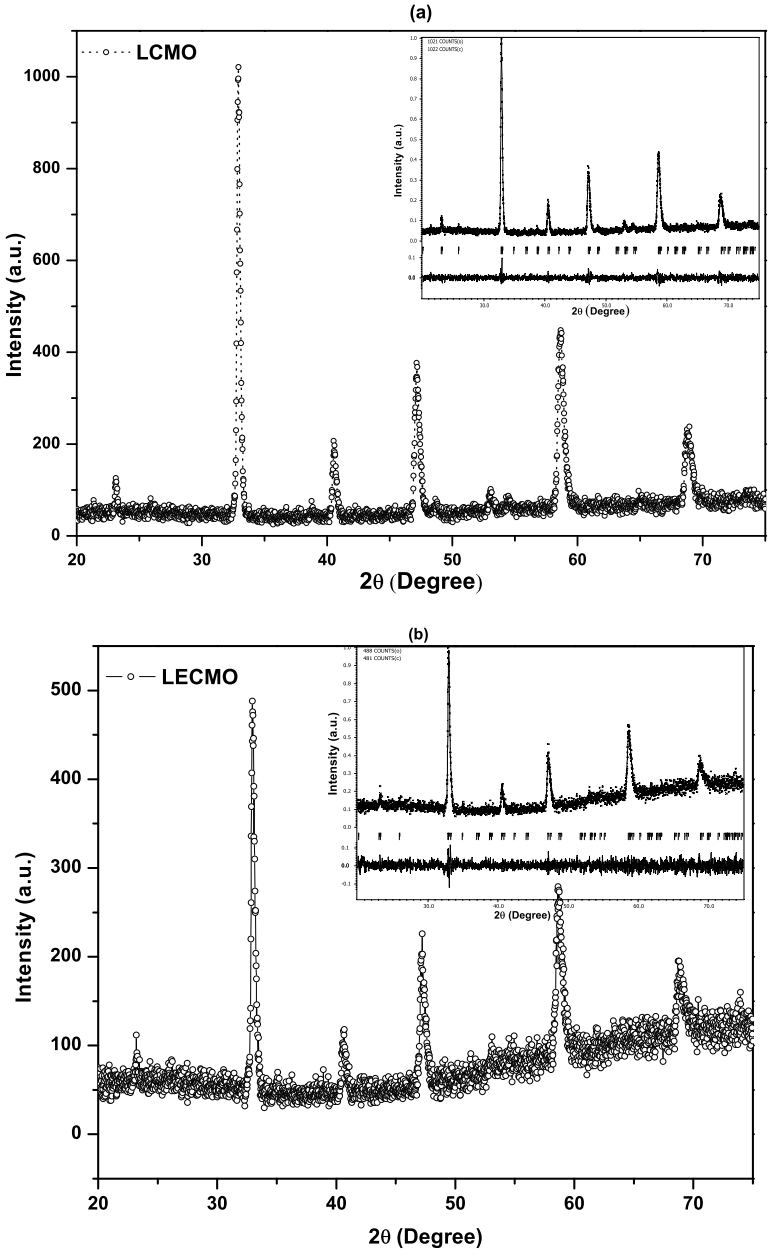

Figure 3.1: XRD patterns of the (a) $La_{0.7}Ca_{0.3}MnO_3$ and (b) $(La_{0.6}Eu_{0.1})Ca_{0.3}$ MnO_3 (b). The insets show the superposition of the observed (dots) and the calculated (line) patterns. The bars just below the patterns are the Bragg positions and the lines at the bottom correspond to the difference.

and uniform grain size with significant pores is formed for both samples that one can observe clear grain boundaries.

Table 3.1: Experimental data of LCMO and LECMO.

Sample	$La_{0.7}Ca_{0.3}MnO_3$	$(La_{0.6}Eu_{0.1})Ca_{0.3}MnO_3$
Sample code	LCMO	LECMO
Ionic radii (Å)	1.216	1.12
a (Å)	5.412(1)	5.379(2)
b (Å)	5.445(1)	5.447(1)
c (Å)	7.711(1)	7.706(1)
V $(Å)^3$	227.2(1)	225.8(1)
$R_p, R_{wp}(\%)$	9.61, 12.54	9.24, 11.80
GOF	1.07	1.08
Space group	Pbnm (No: 62)	Pbnm(No: 62)
T_p (K)	194	165
MR% around T_p for 7 T field	44	47

3.2 Electrical behavior and Magnetoresistance

The evolution of the resistivity with temperature under different magnetic applied fields is plotted in Figure 3.3 [23]. Both samples are found to exhibit a metal-insulator transition in the studied temperature range. Compliant with other systems previously studied [19, 73, 74], the metal-insulator transition temperature T_p is found to decrease with Eu doping from 194 to 165 K (Table 3.1). Also and as it can be seen from the same figure, the resistivity of the doped sample is twice larger than that of the undoped one. This improvement of conductivity could be associated to a successive substitution of Eu^{3+} at A-site (La^{3+}) which reduces the value of $< r_A >$. Consequently, $< r_A >$ becomes too small to fill the space in the cube centers, and the oxygen tends to move towards the center, reducing the d_{A-O} and d_{Mn-O} bond distances. This leads to a distortion in the lattice, and further a deviation in the Mn−O−Mn bond angle (θ) from 180° which provides a local trap for e_g electrons, possibly causing phase or domain separation. Moreover, the hopping amplitude of charge carriers between Mn^{3+} and Mn^{4+} naturally decreases as θ becomes smaller than 180°, leading to local lattice distortions of the MnO_6 octahedra. By consequence, the tendencies of charge localization increase due to the reduction in the mobility of the carriers. Due to that, the value of T_p is expected to decrease with decreasing $< r_A >$ [73, 75].

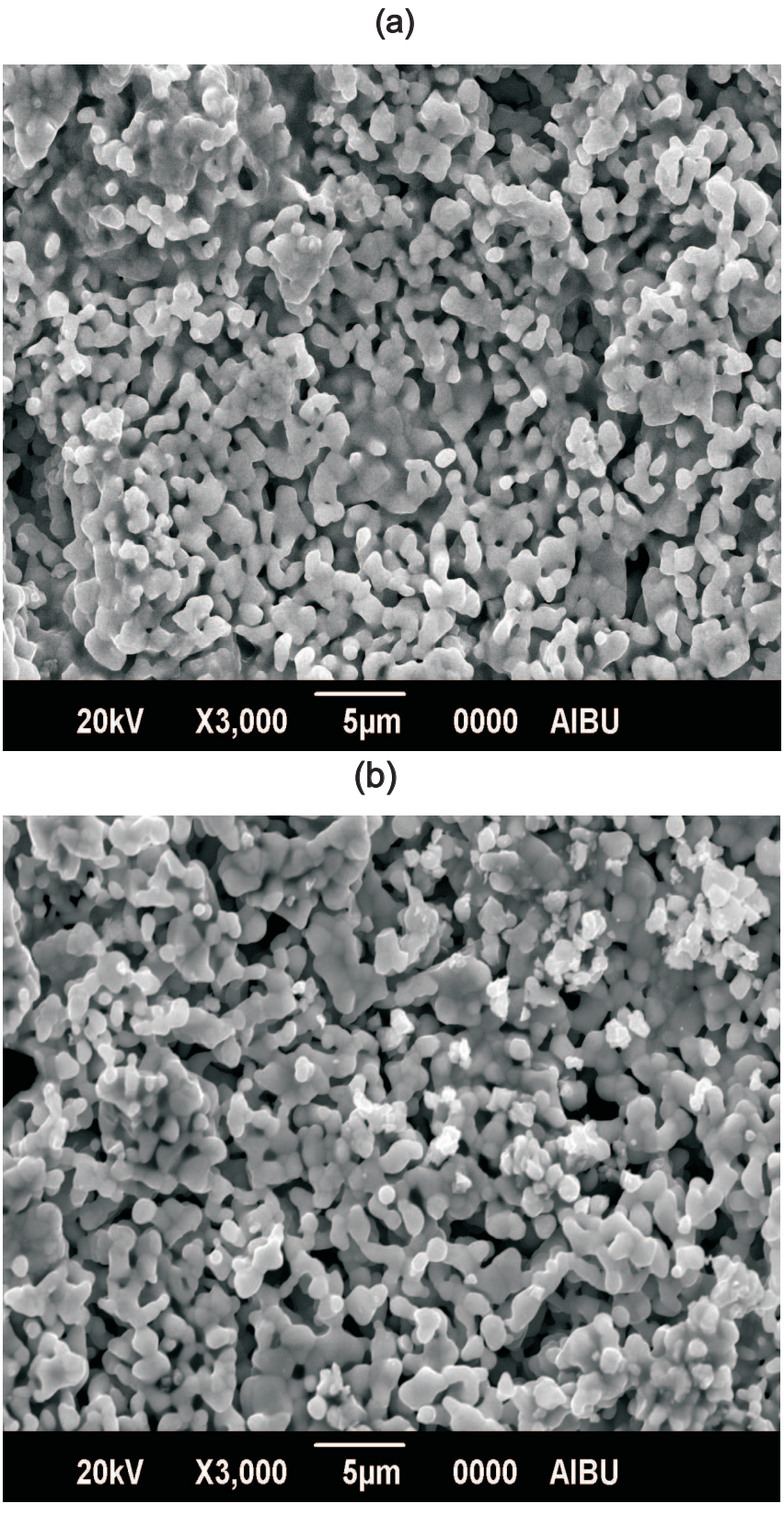

Figure 3.2: SEM images of LCMO (a) and LECMO (b).

In zero field measurements of resistivity one can see from Figure 3.4 [23] that with decreasing temperature, the resistivity (ρ) increases up to metal-insulator

transition temperature (T_p) and then decreases on further decrease of temperature and finally reaches a minimum value at about 20 K for LECMO and 24 K for LCMO. On further decrease of temperature below T_{min}, ρ is found to increase rapidly and the behaviour is a characteristic feature of an insulator [76]. In contrast with the normally observed metallic behaviour in the ferromagnetic region, the samples of present investigations are found to exhibit insulating behaviour. An obvious example can be seen in the insets of Figure 3.4 for 0 T. In fact a similar type of behaviour was reported earlier in other kinds of materials [29, 77, 78]. Moreover, when the magnetic field is increased from 0 to 7 T, the maximum of the resistivity decreases from 21.5 to 11.8 $\Omega.cm$ and from 9.7 to 5.5 $\Omega.cm$ for LECMO and LCMO, respectively. At the same time, the transition temperature T_p shifts towards high temperature region by an amount of 10 K for both samples. This may be due to the fact that the applied magnetic field delocalizes the charge carriers by causing local ordering of the electron spins. Due to this ordering, the ferromagnetic metallic (FMM) state might have suppressed the paramagnetic insulating (PMI) regime resulting in increasing T_p values under the influence of magnetic field [79]. Further, T_{min} is found to shift towards low temperature region with increasing magnetic field. The resistivity upturn below T_{min} is also found to suppress with increasing magnetic field. The origin of this resistivity minimum at low temperatures could be associated to competition between the weak localization effect, electron-electron scattering process and electron-phonon scattering process [80].

As the MR is a fundamental property of manganites, its percentage of the samples has been calculated using Eq. 1. Its evolution with temperature under an applied magnetic field of 7 T is shown in Fig. 3.5 [23]. The obtained values around T_p are given in Table 3.1. For both samples, the largest MR is observed around T_p and remains still remarkable even at the lowest temperatures. A maximum of 47% and 44% is obtained for the doped and undoped samples, respectively. The doping with Eu increases the magnetoresistance of $La_{0.7}Ca_{0.3}MnO_3$ system

which is consistent with the same content of yttrium doped system [18].

Figure 3.6 [23] shows the variation of MR as a function of the applied magnetic field (from -4 to 4 T) at different temperatures. At low temperatures ($\leq 100\ K$), the MR in the field below 1 T increases sharply with the increase of the applied field and shows the general behaviour of the polycrystalline samples with a large low-field MR [81, 82]. After this value ($H > 1\ T$), a slower variation of MR with H is observed. On the contrary, the variation of MR with H is quasi-linear at high temperatures. At 4 T and for all temperatures below T_p, the doped sample exhibits the highest value of MR.

3.2.1 Low-temperature behavior

In spite of nearly two decades of intense work on CMR materials, the variation of resistivity at low temperatures ($T < T_p$) and relative strengths of the different scattering mechanisms originating from different contributions are not yet understood throughly. Therefore, in order to explain the origin of the low temperature resistivity upturn, the experimental data have been analyzed using the following empirical equation [25].

$$\rho(T) = \rho(0) + \rho_2 T^2 + \rho_{4.5} T^{4.5} + \rho_e T^{1/2} - \rho_s lnT + \rho_p T^5 \tag{3.1}$$

where ρ_0 arises due to grain or domain boundaries. As the polycrystalline materials contain grains, grain boundaries and their significant contribution to the resistivity is proved in microwave measurements [83] and hence term ρ_0 will play a major role in the conduction process. On the other hand $\rho_2 T^2$ indicates the electron-electron scattering, while $\rho_{4.5} T^{4.5}$ is attributed to two magnon scattering processes. The last three terms are based on strong correlated effect in manganites; $\rho_e T^{1/2}$ takes care of the contributions from correlated electron-electron interactions, while $\rho_s lnT$ represents the contributions due to Kondo-like spin de-

pendent scattering. $\rho_p T^5$ term is due to electron-phonon interactions. The experimental resistivity data of present investigation were fitted to Eq. 2 and the best fit figures at 0 T and 7 T are shown in Figure 3.7 [23]. It can be seen from the figures that the theoretical and the experimental curves match well. The fit parameters obtained for both curves are tabulated in Table 3.2. One finds from the table that all the parameters are found to decrease with increasing magnetic field (except ρ_s for LCMO) whereas they all increase with Eu doping. The observed behaviour may be explained as follows: When the magnetic field increases, the domain enlarges reducing the value of ρ_0. This may be related to the intrinsic properties of the system and does reflect *CMR* effect and disorder characteristics for the manganite system [81]. The reduction in ρ_2 and $\rho_{4.5}$ could be attributed to decrease in electron spin fluctuations in the presence of magnetic field. The increase in the last three terms indicates that the weak localization, electron-electron and electron-phonon scattering increase with Eu-doping, wherein disorder increases and the material becomes disordered.

Table 3.2: Best fit parameters of low temperature resistivity data.

Sample code	$\rho_0(\Omega.cm)$		ρ_2 x $10^{-6}(\Omega.cm/K^2)$		$\rho_{4.5}$ x $10^{-9}(\Omega.cm/K^{4.5})$	
	0 T	7 T	0 T	7 T	0 T	7 T
LCMO	1.96153	1.33255	34.8501	34.5014	2.70948	1.98308
LECMO	4.06633	2.66228	11.8577	9.27109	9.60308	5.28103
	$\rho_e(\Omega.cm/K^{1/2})$		$\rho_s(\Omega.cm)$		ρ_p x $10^{-10}(\Omega.cm/K^5)$	
	0 T	7 T	0 T	7 T	0 T	7 T
LCMO	0.165863	0.164143	0.309403	0.349267	1.58392	1.23866
LECMO	0.446547	0.278124	0.805593	0.626395	5.61911	3.31422

3.2.2 High-temperature behaviour

In order to explain the variation of electrical resistivity with temperature in the high temperature insulating (semiconducting) regime (above the metal-insulator transition temperature T_p), the resistivity data is fitted by the adiabatic small polaron hopping (PH) model [64]. According to this model the expression of resistivity is given by the relation;

$$\rho/T = \rho_\alpha exp(E_A/k_BT), \tag{3.2}$$

where, E_A represents the activation energy and $\rho_\alpha = 2k_B/3ne^2a^2\nu$ is the residual resistivity. Here k_B is Boltzmann's constant, e is the electronic charge, n is the density of charge carriers, a is site-to-site hopping distance, and ν is longitudinal optical phonon frequency. The resistivity curves of the samples are plotted as $ln(\rho/T)$ versus $(1/T)$ at 0 and 7 T [Fig. 3.8] [23]. Applying the PH model, we have calculated the values of activation energy E_A, and the fitting parameters for this model are presented in Table 3.3. One can see from the table that the activation energies are decreased by application of the magnetic field. This behaviour may be attributed to a reduction of the charge localization.

Table 3.3: Fitting parameters of the PH model for LCMO and LECMO.

Sample code	H (T)	R^2	E_A (meV)	ρ_α x 10^{-6} $(m\Omega cm/K)$
LCMO	0	0.9990	150.39	17.288
	7	0.9942	131.84	33.765
LECMO	0	0.9996	158.65	8.4943
	7	0.9988	143.97	14.658

3.2.3 Conduction mechanism: A new Approach

Many attempts were made to explain the variation of the electrical resistivity with temperature in the case of CMR manganites. Various scattering mechanisms such as electron-electron, electron-magnon and magnon-magnon scattering processes were proposed to explain the low temperature electrical behavior (be-

low T_p). In the high temperature (above T_p) region, thermal activation process, hopping motion of small polarons and variable range hopping mechanism etc., were fitted. The above mentioned models do not fit the resistivity data especially in the vicinity of metal-insulator transition temperature. In order to elucidate the transport mechanism in the entire temperature region, we attempt to fit the $\rho - T$ curves according to phenomenological percolation approach.

According to this approach, the total resistivity of the system is considered to be the sum of the resistances of the phase-separated FM and PI parts, and thus the whole resistivity ρ of the system is given by following equations [84]:

$$\rho = \rho_{FM} f + \rho_{PI}(1 - f) \tag{3.3}$$

where ρ_{FM} and ρ_{PI} are the resistivities for the FM and PI regions and f and $(1-f)$ represent the volume fractions of PI and FM regions in the system, respectively. Since there is an energy difference (per unit cell) ΔU between the FM state and PI state, the volume fractions obey a simple two energy-level Boltzman distribution: $f = \frac{1}{1+\exp(\Delta U/k_B T)}$. As the FM state is a spin-ordered state, it is sensitive to the temperature. When temperature increases, some PI region will appear, but the long-range FM order will be kept to a characteristic temperature T_c^{mod} (here T_c^{mod} is a PI-FM transition temperature used in the model and near/equal to T_c). Without loss of generality, we may expand $\Delta U(T)$ around T_c^{mod} to the first order of $(T - T_c^{mod})$ and require that $\Delta U \approx 0$ at $T = T_c^{mod}$. Therefore we may write $\Delta U \approx -U_0(1 - T/T_c^{mod})$ where U_0 is considered as the energy difference for temperature well below T_c^{mod}.

As known, in the metallic conducting temperature region well below T_p, the metallic resistivity can be ascribed to the residual resistivity ρ_0, single magnon's scattering contribution $\rho_2 T^2$ and electron-phonon interactions $\rho_p T^5$. However, in order to explain the low temperature resistivity upturn, some other factors might have also contributed to the low temperature behavior such as correlated electron-electron interactions $\rho_e T^2$, Kondo-like spin dependent scattering $\rho_s lnT$

and two magnon scattering process $\rho_{4.5}T^{4.5}$. Thus we can represent the ρ_{PI} as:

$$\rho_{PI} = \rho(0) + \rho_2 T^2 + \rho_{4.5} T^{4.5} + \rho_e T^{1/2} - \rho_s lnT + \rho_p T^5 \tag{3.4}$$

In the semiconducting-like region above T_p, the resistivity can be described by the adiabatic small polaron hopping mechanism [25, 85] according to the following formula:

$$\rho_{FM} = \rho_\alpha T \exp E_g/k_B T \tag{3.5}$$

in terms of a magnetic polaron picture.

The fit parameters obtained from *Eqs.* 3.2, 3.3 and 3.4 are tabulated in Table 3.2 for pure sample and the superposition of the experimental and the calculated curves of $\rho(T)$ is shown in Figure 3.9. It can be found that the model yields quantitative fits to the experimental data in the whole temperature range studied both in the presence and absence of magnetic fields for both samples. As a result, T_c^{mod} is close to the T_{MI}. These agreements confirm that FM and PI regions coexist near T_{MI}. It is also clear from the table that the activation energies are found to decrease with increasing magnetic field and the observed behavior may be attributed to the decrease in the values of charge localization under the influence of magnetic field [75].

Table 3.4: Parameters used to fit the experimental data of LCMO compound according percolation aproach.

LCMO			
	$\rho_0(\Omega.cm)$	$\rho_2(\Omega.cm/K^2)$	$\rho_{4.5}$ x $10^{-9}(\Omega.cm/K^{4.5})$
0 T	1.9615	0.00003485	2.7094
0.5 T	1.7377	0.00006017	2.6175
2 T	1.7991	0.00007936	2.4281
4 T	1.3472	0.00003062	1.5334
7 T	1.3111	0.00000832	1.6723
	$\rho_e(\Omega.cm/K^{1/2})$	$\rho_s(\Omega.cm)$	ρ_p x $10^{-10}(\Omega.cm/K^5)$
0 T	0.16586	0.30940	1.5839
0.5 T	0.2624	0.48071	1.5157
2 T	0.36619	0.72808	1.4055
4 T	0.02316	0.09359	9.0311
7 T	0.11922	0.27820	1.0359
	ρ_α x $10^{-4}(\Omega.cm)$	T_c^{mod} (K)	E_g/k_B
0 T	7.3025	206	728.3
0.5 T	5.6208	207.7	670.7
2 T	10.601	210	558.6
4 T	9.5998	211.5	570.6
7 T	20.070	210	500.5

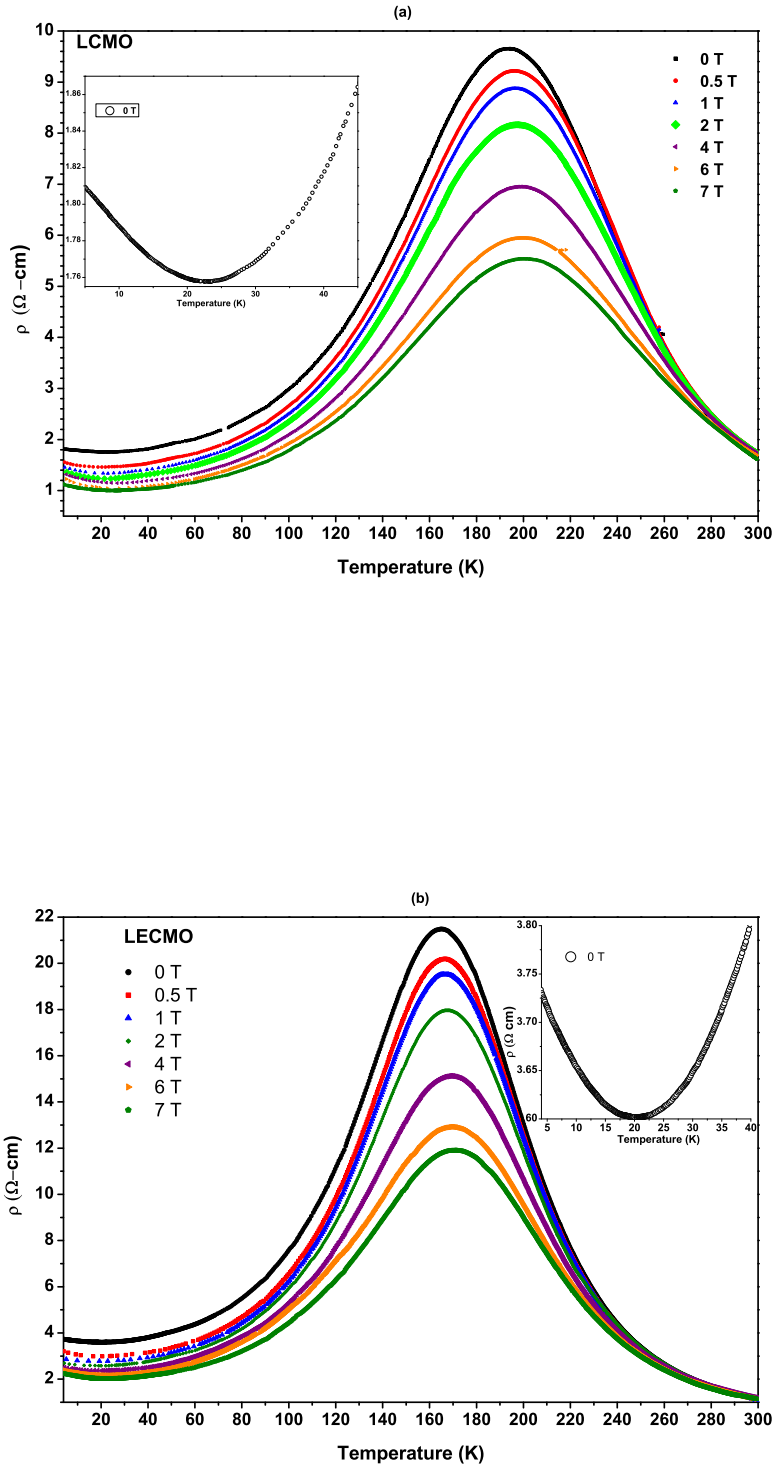

Figure 3.3: Temperature dependence of resistivity under different magnetic fields for LCMO (a) and LECMO (b).

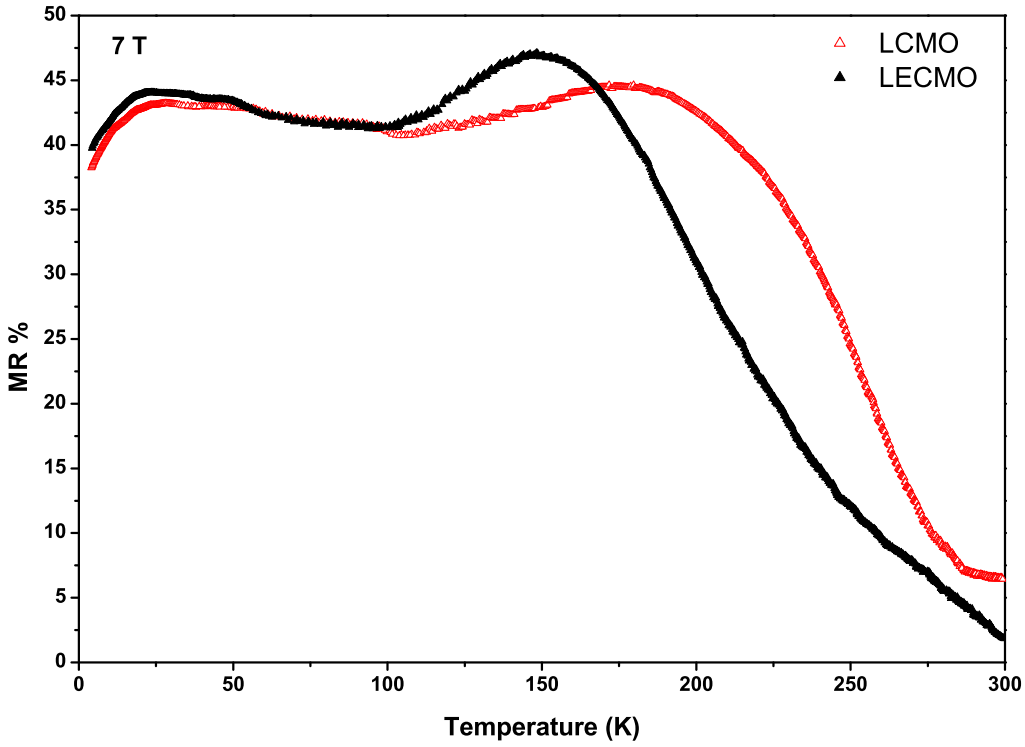

Figure 3.4: MR vs. temperature plots of the LCMO (red line) and LECMO (black line) samples in a field of 7 T.

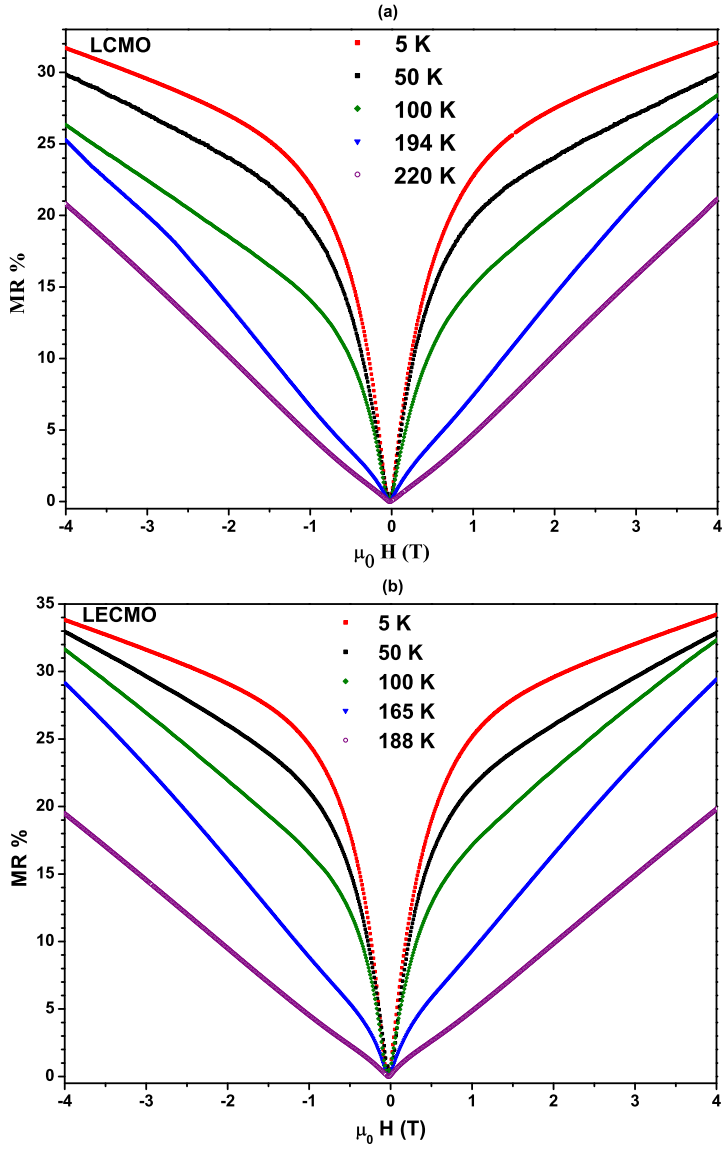

Figure 3.5: MR % vs. magnetic field at different temperatures for LCMO (a) and LECMO (b).

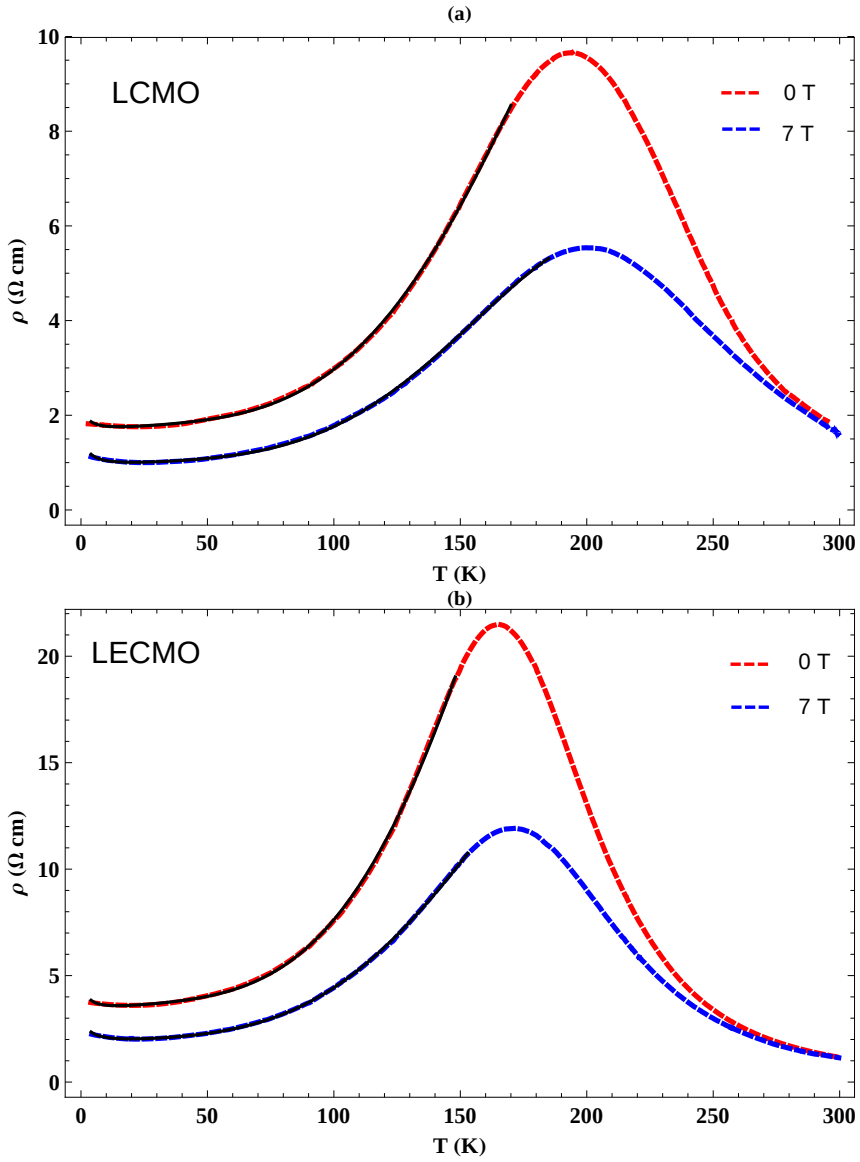

Figure 3.6: Theoretical fit of low temperature resistivity data for LCMO (a) and LECMO (b).

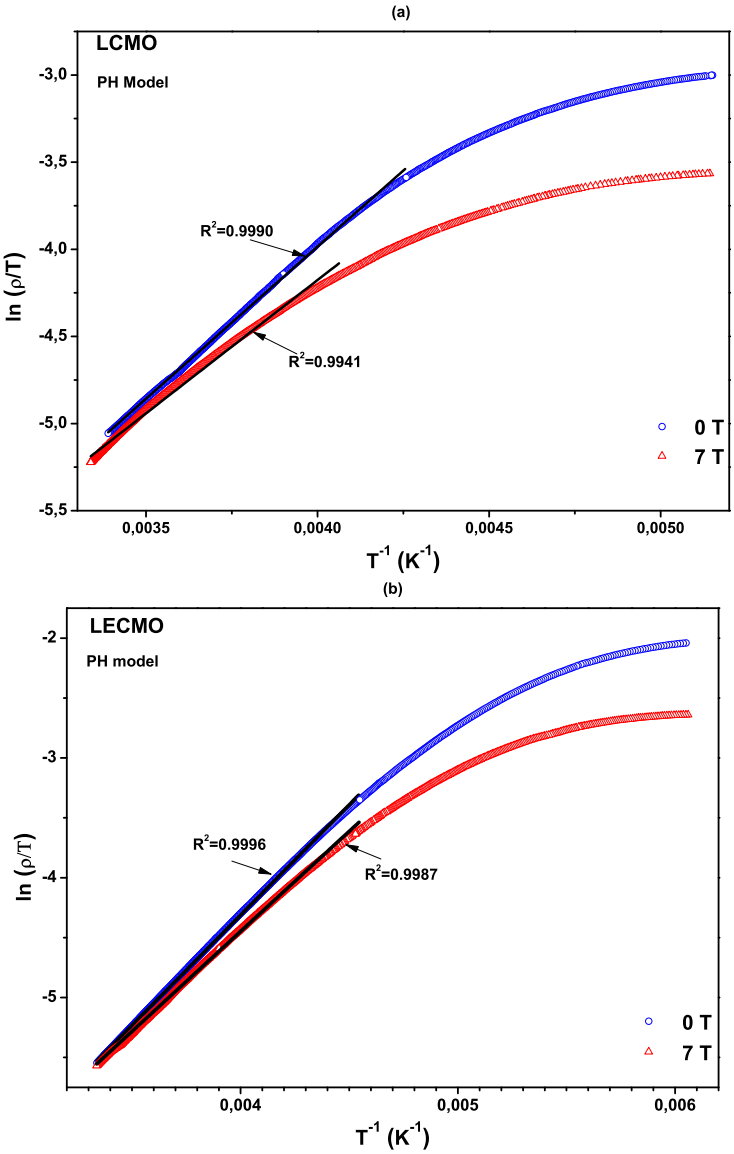

Figure 3.7: Theoretical fit of high temperature resistivity data for LCMO (a) and LECMO (b).

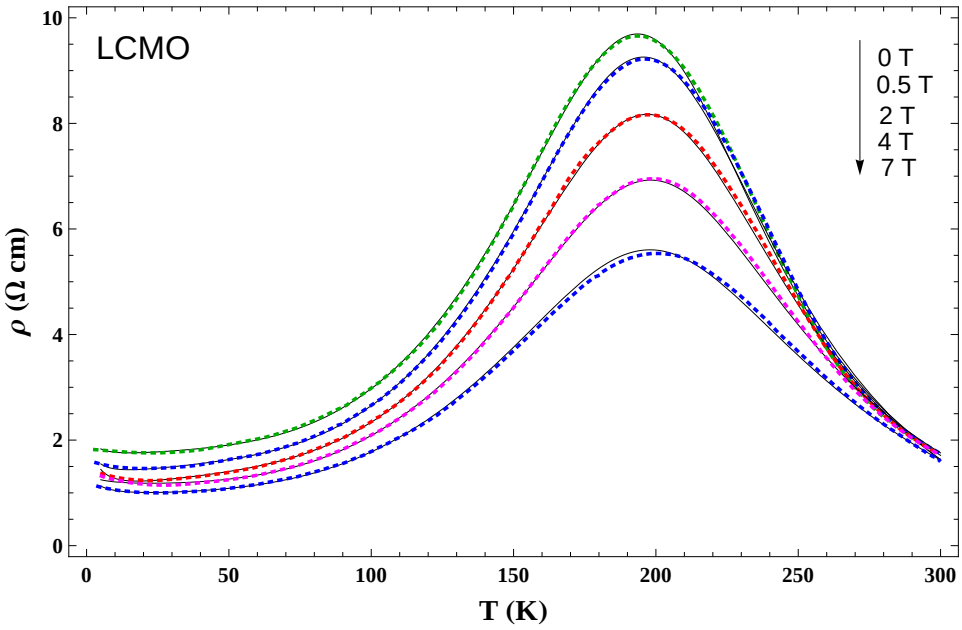

Figure 3.8: Comparison between the calculated (solid lines) and experimental (dashed) temperature dependencies of resistivity in different magnetic fields up to 7 T for $La_{0.7}Ca_{0.3}MnO_3$.

CHAPTER 4

CONCLUSION

In summary, the structural and magneto-electrical properties of bulk ($La_{0.7-x}Eu_x$) $Ca_{0.3}MnO_3$ (x=0 and 0.1) samples are presented. The Eu doping causes a decrease of the metal-insulator transition temperature T_p from 194 to 165 K and makes the resistivity twice larger. A maximum of magneto-resistance of 44% and 47% is observed at a magnetic field of 7 T for the undoped and doped samples, respectively. Moreover, these values are observed around their T_p and remains still remarkable even at the lowest temperatures. It has also been concluded that the electrical conduction mechanism at low temperatures ($T < T_p$) can be explained by a theory based on Kondo-like spin dependent scattering, electron-electron, electron-phonon and electron-magnon scattering while the adiabatic small polaron hopping machanism can be used in the high temperature ($T > T_p$) regime.

REFERENCES

[1] J. M. D. Coey, M. Viret, S. von Molnar, Adv. Phys. **48**, (1999) 167 .

[2] D. H. Manh, P. T. Phong, T. D. Thanh, L. V. Hong, and N. X. Phuc, J. Alloys Compd. **491**, (2010) 8.

[3] P. K. Siwach, H. K. Singh, O. Srivastava, J. Phys.: Condens. Matter **20**, (2008) 273201.

[4] Md. M. Seikh, L. Sudheendra, C. N. R. Rao, J. Solid State Chem. **177**, (2004) 3633.

[5] J. Mira, J. Rivas, L. E. Hueso, F. Rivadulla, M. A. López Quintela, M. A. Señarís Rodríguez, and C. A. Ramos, Phys. Rev. B **65**, (2001) 024418.

[6] L. Hueso, N. D. Mathur, Nature **427**, (2004) 303.

[7] S. L. Yuan, J. Q. Li, Y. Jiang, Y. P. Yang, X. Y. Zeng, G. Li, F. Tu, G. Q. Zhang, C. Q. Tang, and S. Z. Jinet, Phys. Rev. B **62**, (2000) 5313.

[8] M. T. Causa, M. Tovar, A. Caneiro, F. Prado, G. Ibanez, C. A. Ramos, A. Butera, B. Alascio, X. Obradors, S. Pinol, F. Rivadulla, C. Vazquez-Vazquez, M. A. Lopez-Quintela, J. Rivas, Y. Tokura, and S. B. Oseroff, Phys. Rev. B **58**, (1998) 3233 .

[9] C. Zener, Phys. Rev. **81**, (1951) 440.

[10] C. Sen, G. Alvarez, E. Dagotto, Phys. Rev. B **70**, (2004) 064428.

[11] L. Pi, M. Hervieu, A. Maignan, C. Martin, B. Raveau, Solid State Commun. **126**, (2003) 229.

[12] N. Panwar, V. Sen , D. K. Pandya, S. K. Agarwal, Materials Letters **61**, (2007) 4879.

[13] A. J. Millis, P. B. Littlewood and B. I. Shraiman, Phys. Rev. Lett. **74**, (1995) 5144.

[14] A. P. Ramirez, J. Phys.: Condens. Matter **9**, (1997) 8171.

[15] P. G. de Gennes, Phys. Rev. **118**, (1960) 141.

[16] J. M. DeTeresa, J. Blasco, M. R. Ibarra, J. Garcia, C. Marguina, P. Algarabel and A. del Moral, Solid State Commun. **96**, (1995) 627.

[17] H. Y. Hwang, S. W. Cheong, P. G. Radaelli, M. Marezio, and B. Batlogg, Phys. Rev. Lett. **75**, (1995) 914 .

[18] G. M. B. Castro, A. R. Rodrigues, F. L. A. Machado, A. E. P. de Araujo, R. F. Jardim, A. K. Nigam, J. Alloys Compd. **369**, (2004) 108.

[19] T. G. Reddy, P. Y. Reddy, V. R. Reddy, A. Gupta, M. Gupta, K. R. Reddy, Solid State Commun. **133**, (2005) 77.

[20] G. H. Zheng, Z. X. Dai, Y. Y. Zhang and Y. P. Sun, J. Alloys Compd. **489**, (2010) 348.

[21] M. Mazaheri, M. Akhavan, J. Magn. Magn. Mater. **322**, (2010) 3255.

[22] J. H. Hao, Z. S. Li, and H. K. Wong, Mater. Sci. Eng. B, **83** (2001) 70.

[23] S. P. Altintas, A. Amira, N. Mahamdioua, A. Varilci and C. Terzioglu, J. Alloys Compd. **509** (2011) 4510.

[24] E. Syskasis, G. Choudalakis and C. Papastaikoudis, J.Phy.: Condens. Matter **15**, (2003) 7735.

[25] M. Ziese, Phys. Rev. B **68**, (2003) 132411.

[26] D. Kumar, J. Sankar, J. Narayan, R. K. Singh, and A. K. Majumdar, Phys. Rev. B **65**, (2002) 094407.

[27] T. Okuda, T. Kimura and Y. Tokura, Phys. Rev. B **60**, (1999) 3370.

[28] N. V. Khiem, P. T. Phong, N. V. Dai, H. D. Chinh, D. H. Manh, L. V. Hong, N. X. Phucet, Mater. Lett. **63**, (2009) 899.

[29] E. Rozenberg, M. Auslender, I. Felner, G. Gorodetsky, J. Appl. Phys. **88**, (2000) 2578.

[30] P. Sheng, B. Abeles, Y. Arie, Phys. Rev. Lett. **73**, (2006) 214425.

[31] G. H. Jonker and H. van Santen, Physica **16**, (1950) 337.

[32] H. van Santen and G. H. Jonker, Physica **16**, (1950) 599.

[33] E. O. Wollan and W. C. Koehler, Phys. Rev. **100**, (1955) 545.

[34] J. Volger, Physica **20**, (1954) 49.

[35] J. B. Goodenough and J. M. Longo, in Landolt-Börnstein Tabellen (Springer, Berlin, 1970), Vol. III/4a.

[36] P. W. Anderson and H. Hasegawa, Phys. Rev. **100**, (1955) 675.

[37] S. Zhang, J. Appl. Phys. **79**, (1996) 4542.

[38] A. J. Millis, B. I. Shraiman, and R. Mueller, Phys. Rev. Lett. **77**, (1996) 175.

[39] A. J. Millis, B. I. Shraiman, and R. Mueller, Phys. Rev. B **53**, (1996) 8434.

[40] A. M. Haghiri-Gosnet and J. P. Renard, J. Phys. D: Appl. Phys. **36** (2003) R127.

[41] V. P. S. Awana, R. Tripathi, N. Kumar, H. Kishan, G. L. Bhalla, R. Zeng, L. S. Sharth Chandra, V. Ganesan, and H. U. Habermeier, J. Appl. Phys. **107** (2010) 09D723.

[42] C. B. Alcock, R. C. Doshi, and Y. Shen, Solid State Ionics **51**, (1992) 281.

[43] T. Kobayashi, H. Takizawa, T. Endo, T. Sato, and M. Shimada, J. Solid State Chem. **92**, (1991) 116.

[44] H. Taguchi, M. Nagao, and M. Shimada, J. Solid State Chem. 97, (1992) 476.

[45] J. A. M. van Roosmalen, J. P. P. Huijsmans, and L. Plomp, Solid State Ionics **66**, (1993) 279.

[46] A. Hammouche, E. J. L. Schouler, and M. Henault, Solid State Ionics **28-30**, (1988) 1205.

[47] Y. Tokura, Colossal Magnetoresistive Oxides, Gordon and Breach Science Publishers, Singapore (2000).

[48] D. Louca, T. Egami, E. L. Brosha, H. Röder, and A. R. Bishop, Phys. Rev. B **56**, (1997) R8475.

[49] S. Zhou, J. Xu, S. Li, W. Yang, J. Zou, G. Zhao, H. Li, Y. Hang, J. R. Cheng and Y. Zhang, Phys. Stat. Sol. A, **201**, No. 5, (2004) 990.

[50] M. Lide. R. Martinez and J. P. Attfield, Phys. Rev. B **54**, (1996) R15622.

[51] H. A. Jahn, E. Teller, Proc. Roy. Soc. A **161**, (1937) 220.

[52] S. Mercone, C. A. Perroni, V. Cataudella, C. Adamo, M. Angeloni, C. Aruta, G. De Filippis, F. Miletto, A. Oropallo, P. Perna, A. Yu. Petrov, U. Scotti di Uccio, and L. MaritatoY. Phys. Rev. B **71**, (2005) 064415.

[53] H. A. Kramers, Physica **1**, (1934) 182.

[54] M. Uehara, S. Mori, C. H. Chen and S. W. Cheong, Nature **399**, (1999) 560.

[55] E. Dagotto, S. Yunoki and A. Moreo, Mater. Sci. Eng. B **63**, (1999) 65.

[56] D. Khomskii, Physica B. **280**, (2000) 325.

[57] P. Moschkau, S. Schramm, J. Hoffmann, J. Fladerer, Ch. Jooss, L. Wu and Y. Zhu, Mater. Sci. Eng. B **144**, (2007) 78 .

[58] R. M. Kusters, J. Singleton, D. A. Keen, R. McGreevy and W. Hayes, Physica B **155**, (1989) 362.

[59] G. J. Snyder, R. Hiskes, S. DiCarolis, M. R. Beasley and T. H. Geballe, Phys. Rev. B **53**, (1996) 14434.

[60] M. Viret, L. Ranno and J. M. D. Coey, Phys. Rev. B **55**, (1997) 8067.

[61] N. F. Mott, Clarendon Press, Oxford (1993).

[62] N. F. Mott, J. Non-Cryst. Solids **1**, (1968) 1.

[63] J. C. Loudon, Ph. D. Thesis, University of Cambridge (2003).

[64] M. Ziese and C. Srinitiwarawong, Phys. Rev. B **58**, (1998) 11519.

[65] D. A. Rudman and M. R. Beasley, Appl. Phys. Lett. **36**, (1980) 1010.

[66] R. Meservey, P. M. Tedrow and J. S. Brooks, J. Appl. Phys. **53**, (1982) 1563.

[67] Y. Tokura, Rep. Prog. Phys. **69**, (2006) 797.

[68] A. Moreo, M. Mayer, A. Feiguin, S. Yunoki, E. Dagotto, Phys. Rev. Lett. **84**, (2000) 5568.

[69] D. Saurel, A. Brûlet, A. Heinemann, C. Martin, S. Mercone, C. Simon, Phys. Rev. B **73**, (2006) 094438.

[70] V. Petricek, M. Dusek, L. Palatinus, Jana 2006, The crystallographic computing system, Institute of Physics, Praha, Czech Republic.

[71] ICDD-Powder Diffraction File, 460513, International Centre for Diffraction Data, 12 Campus Boulevard, Newtown Square, PA, USA.

[72] G. R. Turpu, A. Gupta and K. R. Reddy, J. Phys. D: Appl. Phys. **42**, (2009) 145004.

[73] G. Venkataiah, V. Prasad, P. Venugopal Reddy, Solid State Commun. **141**, (2007) 73.

[74] M. Xu, X. Hu, J. Yu, X. Cui and S. Zhang, Solid State Commun. **148**, (2008) 217.

[75] S. Bhattacharya, R. K. Mukherjee, and B. K. Chaudhuri, Appl. Phys. Lett. **82**, (2003) 4101.

[76] S. Jin, T. H. Tiefel, M. McCromack, R. A. Fastnach, R. Ramesh, L. H. Chen, Science **264**, (1994) 413.

[77] M. Auslender, A. E. Karkin, E. Rozenberg, G. Gorodetsky, J. Appl. Phys. **89**, (2001) 6639.

[78] T. Sarkar, B. Ghosh, A. K. Raychaudhuri, and T. Chatterji, Phys. Rev. B **77**, (2008) 235112.

[79] G. Venkataiah and P. V. Reddy, Solid State Commun. **136**, (2005) 114.

[80] L. Li, K. Nishimura, M. Fujii, K. Mori, Solid State Commun. **144**, (2007) 10.

[81] Y. Xu, J. Zhang, G. Cao, C. Jing, and S. Cao, Phys. Rev. B **73**, (2006) 224410.

[82] H. Y. Hwang, S -W. Cheong, N. P. Ong, B. Batlogg, Phys. Rev. Lett. **77**, (1996) 2041.

[83] M. Dominguez, S. M. Bhagat, S. E. Lofland, J. S. Ramachandran, G. C. Xiong, H. L. Ju, T. Venkatesan and R. L. Greene, EuroPhys. Lett. **32**, (1995) 349.

[84] G. Li, H. D. Zhou, S. J. Feng, X. J. Fan, and X. G. Li, J. Appl. Phys. **92** (2002) 1406.

[85] D. Varshney, D. Choudhary and M. W. Shaikh, Comp. Mater. Science **47** (2010) 839.